International Journal of Applied Pharmaceutics

ISSN- 0975-7058 Vol 16, Issue 6, 2024

Original Article

OPTIMIZATION OF PROCESS PARAMETERS FOR ENHANCING THE SKIN PERMEATION EFFICIENCY OF NISOLDIPINE LOADED ULTRA DEFORMABLE VESICLES IN TRANSDERMAL PATCHES

D. MAHESWARA REDDY[1], MOTHILAL M.[2*]

[1]SRM College of Pharmacy, SRM Institute of Science and Technology, Kattankulathur-603203, Tamilnadu, India. [2]Department of Pharmaceutics, SRM College of Pharmacy, SRM Institute of Science and Technology, Kattankulathur-603203, Tamilnadu, India
*Corresponding author: Mothilal M.; *Email: mothilam@srmist.edu.in

Received: 09 Jul 2024, Revised and Accepted: 20 Sep 2024

ABSTRACT

Objective: The study aimed to address the limitations of oral delivery and enhance the bioavailability of nisoldipine (NSD) through the development of transferosomal transdermal patches containing ultra-deformable transferosomes.

Methods: NSD, known for its low oral bioavailability and adverse effects, was encapsulated in transferosomes using a thin film hydration method. 17 formulations were made using Box Behnken Design, varying Dipalmitoylphosphatidylcholine (DPPC), span-80, and stirring speed, and were evaluated for vesicle size, Polydispersity Index (PDI), and Entrapment Efficiency (EE%). The optimal formulation, selected based on these parameters, was combined into Transdermal Patches (TPs). The patches underwent extensive testing for physicochemical properties, *in vitro* and *ex-vivo* permeation, and skin irritancy.

Results: The results showed transferosomes with Vesicle Sizes (VS) ranging from 124±2.25 to 400±1.55 nm and EE% from 52.88±0.23 to 90.01±1.58%, with Zeta Potentials (ZP) between-48 to-20 mV. The patch thickness (0.66±0.02 mm) and weight per square inch (382.1±1.69 mg) showed consistent manufacturing, while the Water Vapor Transmission Rate (WVT) (1.54±0.01g/m^2/24h), low moisture content (1.07±0.01%), and regulated moisture absorption (3.78±0.01%) maintained formulation stability. *In vitro* and *ex-vivo* permeation indicated superior drug permeation for transferosomal patches (NP) compared to plain nisoldipine patches (NP-N), with permeation directly proportional to PEG-400 concentration. Additionally, the transferosomal patches were found to be free from skin irritation.

Conclusion: The optimized Niosoldipine transferosomal patch (NP-3) composition displays good folding endurance (FE) 97.67±0.47, required for transdermal systems, and successfully allows drug permeation (DP) at 86.39±2.64% in a short timescale. Hence, the study concludes that transferosomal patches of NSD offer a promising approach for effective transdermal delivery, potentially improving hypertension management by providing a controlled and prolonged drug release.

Keywords: Drug permeation, Hypertension management, Nisoldipine, Transdermal patches, Transferosomes

DOI: https://dx.doi.org/10.22159/ijap.2024v16i6.52019 Journal homepage: https://innovareacademics.in/journals/index.php/ijap

INTRODUCTION

Nisoldipine (NSD) is a dihydropyridine calcium channel blocker used primarily to manage hypertension and angina pectoris by inhibiting the influx of calcium ions in vascular and cardiac muscle, causing vasodilation and lowering blood pressure [1]. However, its low oral bioavailability and significant first-pass metabolism reduce its effectiveness when taken orally, necessitating higher doses that can increase the risk of adverse effects such as dizziness, flushing, headache, and peripheral edema [2]. To overcome these challenges, alternative delivery methods like transdermal patches and transferosomes are being explored to improve bioavailability and provide a more controlled release of the drug. Transdermal patches, for instance, enable direct absorption through the skin into the bloodstream, potentially enhancing patient compliance, reducing side effects, and ensuring more stable blood pressure control [3]. Ongoing research into these delivery systems aims to enhance the efficacy and safety profile of NSD, making it a more effective option for treating hypertension and angina [4].

Transdermal Patches (TPs) provide a promising alternative for hypertension management, addressing the limitations of traditional oral medications [5]. They offer steady, prolonged drug release, enhancing patient compliance by reducing dosing frequency. By bypassing the gastrointestinal tract and liver, transdermal delivery increases bioavailability and minimizes side effects. Additionally, patches ensure more stable blood pressure control by maintaining consistent plasma drug levels, reducing the risk of adverse cardiovascular events linked to fluctuations. Their convenience and ease of use, especially for elderly patients or those with cognitive impairments, improve patient quality of life [6]. Overall, transdermal patches enhance efficacy, safety, and adherence in hypertension treatment, contributing to better long-term cardiovascular health outcomes.

Transferosomes offer a significant advancement over traditional transdermal patches for drug delivery, particularly in enhancing the permeation and bioavailability of medications [7]. Transferosomes are ultra-flexible vesicles composed of phospholipids and edge activators, which enable them to deform and pass through the narrow pores of the skin more effectively than conventional patches [8]. This enhanced permeation capability allows for the delivery of larger and more complex drug molecules, including those with poor solubility. Furthermore, transferosomes provide a more controlled and sustained release of drugs, improving therapeutic outcomes and reducing the frequency of dosing. The flexibility of transferosomes also minimizes skin irritation and maximizes patient comfort. Their ability to target specific tissues and achieve higher drug concentrations at the desired site makes them particularly beneficial for conditions requiring localized treatment [9]. Overall, transferosomes represent a superior drug delivery system, offering improved efficiency, patient compliance, and therapeutic effectiveness over traditional transdermal patches [10-12].

This study aims to formulate nisoldipine transferosomes using the Box-Behnken design method. Subsequently, optimized formulations will be developed into TPs. The efficacy and characteristics of these patches will then be thoroughly evaluated.

MATERIALS AND METHODS

Materials

Cipla, Bangalore, generously provided nisoldipine. Dipalmitoylphosphatidylcholine (DPPC), Span-80, and PEG 400 were

acquired from Loba Chemie Pvt. Ltd., Mumbai. All other reagents used were of analytical grade.

Preparation of NSD transferosomes

DPPC and span-80 were dissolved in a mixture of chloroform and ethanol (2:1 ratio). The solvent was removed using rotary evaporation for 15 min followed by overnight vacuum drying to eliminate any residual solvent. The lipid films thus formed were reconstituted by hydrating them with 10 ml of phosphate buffer at pH 6.8 containing NSD. The hydration process involved rotating the mixture for 45 min. The resulting transfersomal suspension was stored refrigerated at 4 °C [13, 14]. A total of 17 formulations were made using the Box-Behnken Design method facilitated by Design Expert software (table 1).

Table 1: Composition of NSD transferosomes

Independent variables	Levels		
	Low	Medium	High
X_1= DPPC (mg)	50	85	120
X_2= span-80 (mg)	15	20	25
X_3= stirring speed (rpm)	60	70	80
Transformed values	-1	0	+1
Dependent variables	Goals		
Y_1= Vesicle size	Minimize		
Y_2= entrapment efficiency	Maximize		
Y_3= Zeta potential	Above ±25 mv		

Compatibility

Differential Scanning Calorimetry (DSC) and Fourier-Transform Infrared Spectroscopy (FTIR) Spectroscopy were employed to evaluate the compatibility between the NSD and polymers. DSC analysis involved heating samples of the NSD alone and in combination with excipients from 30-300 °C to observe changes in thermal properties such as melting points and enthalpy, which indicate potential interactions. By comparing the DSC thermograms of the NSD and its mixtures, any shifts or changes provide evidence of compatibility or incompatibility, ensuring that the polymers do not negatively impact the NSD's stability and efficacy. FTIR spectroscopy analyzed chemical bonds and functional groups in the NSD and polymers, capturing spectra from 4000 to 400 cm^{-1}. This analysis revealed interactions at the molecular level by identifying characteristic peaks, shifts, and changes in peak intensity, indicating bond interactions or the formation of new bonds. Together, DSC and FTIR spectroscopy offer a comprehensive evaluation of the thermal and chemical compatibility of the NSD with the polymers, ensuring the stability and efficacy of the final product.

Optimization

In this study, the interaction effects of DPPC and span-80 on nisoldipine transferosomes (NT) were evaluated using a Box-Behnken design. Design-Expert software generated 17 experimental runs based on a nonlinear computer-generated quadratic model equation. This equation considered the response (Y) linked to each combination of factor levels, incorporating linear coefficients (b_1, b_2, b_3), interaction coefficients (b_{12}, b_{13}, b_{23}), and quadratic coefficients (b_{11}, b_{22}, b_{33}), with b_0 as the intercept. The Independent Variables included phospholipid (X_1), surfactant (X_2), and stirring speed (X_3), while Vesicle Size (VS) (Y_1), Entrapment Efficiency (EE%) (Y_2), and Zeta Potential (ZP) (Y_3) served as dependent variables [15]. The chosen range of IVs was determined based on preliminary trials, with each variable studied at three levels: low (-1), medium (0), and high (+1). This comprehensive approach enabled a systematic investigation into the optimal formulation conditions for producing NT with desired characteristics [16, 17].

Description of NTs

Vesicle size, polydispersity index (PDI), and ZP

To characterize the transferosomal suspension, a series of analyses were conducted to determine key parameters influencing its stability and behavior. To assess the VS and surface charge (ZP), a sample of the transferosomal suspension was first diluted with double-distilled water to ensure optimal measurement conditions. Subsequently, the VS and ZP were measured using a laser scattering particle size analyzer [18, 19].

Entrapment efficiency

To determine the EE % of NSD transferosomal suspensions, ultracentrifugation is initially performed at 20,000 rpm and 10 °C for 30 min [20]. Following centrifugation, 1 ml of the supernatant is extracted and diluted with 9 ml of phosphate saline buffer (pH 7.4). Subsequently, the absorbance of the diluted supernatant is measured at 237 nm using a UV-Vis spectrophotometer (Thermo Spectronic UV-1, USA) (E. q.1) [21].

$$\text{EE (\%)} = \frac{\text{(Total NSD taken} - \text{Free NSD)}}{\text{Total NSD taken}} \text{X100 --- (1)}$$

Deformability

The Deformability Index (DI) of vesicles is a measure that quantifies the change in VS or morphology before and after a deformative process, such as extrusion. It provides insights into the ability of vesicles to deform and adapt to different environments, which is crucial for their effectiveness in drug delivery applications, particularly across biological barriers like the skin. The vesicles underwent passage through a 50 nm polycarbonate membrane using an extruder. Both before and after extrusion, the vesicles were analyzed for VS, elasticity, and DI. VS was determined using dynamic light scattering (DLS). Elasticity was quantified by dividing the VS after extrusion by the mesh size of the membrane [22, 23]. The deformability index was calculated by comparing VS before and after extrusion (e. q.2).

$$\text{DI} = \frac{\text{D (initial)} - \text{D (final)}}{\text{D(initial)}} \text{X100 --- (2)}$$

Confocal laser scanning microscopy (CLSM)

CLSM was utilized to investigate the penetration of elastic liposomal formulations through the skin. These NTs were loaded with an NSD fluorescent probe, allowing for visualization under fluorescence microscopy. Before the CLSM study, a skin penetration analysis was led. NSD-labeled vesicles were applied to skin mounted on Franz cells, and after an 8-hour treatment period, the skin was mildly washed, and the treated area was excised. Subsequently, the skin was frozen at-60 °C and sectioned vertically using a mechanical device to obtain samples with a thickness of 10 µm. The analysis was performed using CLSM at 543 nm and an emission wavelength of 560 nm specific to the NSD probe [24-26]. This methodology allowed for the visualization and examination of the penetration of the fluorescently labeled vesicles across diverse layers of the skin, providing insights into their worth and distribution for potential therapeutic applications [27].

The Optimized Transferosomal Formulation (NT-3) showed lesser VS, better ZP, and EE%. So, it was further incorporated and made into TPs.

Preparation of NSD transdermal films

A magnetic stirrer was utilized (at a slow speed) to dissolve precise amounts of HPMC E5 and ethyl cellulose in a 1:1 mixture of methanol and dichloromethane solvents. To these methylparaben and NT-3 were added and stirred at 100 rpm and maintained at 25 °C (to get nisoldipine patches and named them as NP-3), the prepared mixture was spread onto Petri dishes greased with glycerine and then subjected to a one-hour exposure in a 40 °C oven. Subsequently, the NP-3 patches were enveloped in a fabric backing film composed of Ethylene-Vinyl Acetate (EVA). The adhesive side of the NP-3 was shielded by a liner made of Poly Vinyl Pyrrolidone (PVP). Finally, the completed NP-3 patches were stored in a desiccator until ready for use [28-30].

Evaluation studies of NP-3

The evaluation of NP-3 involves a comprehensive assessment of various physicochemical parameters to ensure the quality, consistency, and efficacy of these drug delivery systems. Below is a detailed description of each evaluation parameter.

Thickness measurement

Utilizing a digital screw gauge, the thickness of NP-3 patches is meticulously assessed at various points to ensure consistency and reliability. This detailed measurement process is crucial for confirming uniformity throughout the patches and plays a critical role in evaluating the overall structural integrity of NP-3. By systematically measuring the thickness across multiple points, any variations can be identified and addressed, ensuring that NP-3 meets rigorous quality standards for its intended applications as a drug delivery system [31, 32].

Weight variation analysis

To ensure uniformity in the distribution and composition of NSD within NP-3 patches, ten randomly selected patches are dissected into sections, and the weight of each section is individually measured. This meticulous process enables the calculation of average weight and standard deviation across the patches, ensuring consistency in the composition of each patch. By analysing multiple sections from each patch, any variability in NSD distribution can be identified and controlled, thereby confirming the reliability and quality of NP-3 as a drug delivery system [33, 34].

NSD content assessment

A precise section of the TP (200 mg) is dissolved in a specific volume of phosphate buffer solution. This solution undergoes continuous shaking in a shaker incubator and subsequent sonication to ensure thorough dissolution of the NSD. Following dissolution, the solution is filtered and appropriately diluted. The NSD content in the resulting solution is quantified using a UV-visible spectrophotometer at a predetermined wavelength, typically 237 nm. This analytical method allows for accurate measurement of the NSD concentration, ensuring precise determination of drug content in the TP formulation [35, 36].

Moisture content

The moisture content of transdermal NP-3 is evaluated to ensure its stability and longevity. Each batch is individually weighed and placed in a desiccator containing activated silica. Over 24 h, the NP-3 samples are periodically reweighed until a constant weight is achieved, indicating that equilibrium with the desiccant has been reached. The percentage moisture content is then calculated based on the initial and final weights of each sample, providing critical data on the moisture levels present in the formulation. This meticulous process helps in maintaining the quality and effectiveness of NP-3 by ensuring that moisture levels are controlled within acceptable limits for transdermal applications [37, 38].

Assessing the moisture uptake

To evaluate the moisture absorption capacity of NP-3, samples are initially weighed and placed in a desiccator containing a saturated solution of KCl for 24 h. During this period, the NP-3 samples absorb moisture from the environment. Subsequently, the samples are repeatedly weighed until a constant weight is achieved, indicating that equilibrium with the ambient moisture has been reached. The percentage moisture uptake is then calculated based on the difference between the initial and final weights of each sample [39]. This method provides insights into the formulation's ability to absorb moisture under controlled conditions, essential for assessing its stability and performance in real-world environmental conditions [40].

Flatness testing

The flatness of transdermal NP-3 patches is assessed to ensure they maintain a smooth surface and do not deform over time. Strips are cut from the center and both ends of each NP-3 patch, and their lengths are measured. Any variation in length between the center and ends of the patch, which indicates non-uniformity in flatness, is quantified as a percentage constriction [41]. This method allows for the precise evaluation of patch integrity and ensures that NP-3 patches maintain consistent physical characteristics necessary for effective transdermal drug delivery [42].

Assessing the folding endurance (FE)

The FE of NP-3 is determined by repetitively folding a small section of the patch at the same location until it develops a crack. The number of folds completed before crack formation specifies the FE value, which reflects the flexibility and durability of the patch material [43]. This method assesses the ability of NP-3 to withstand repeated stress and folding without compromising its structural integrity, ensuring its suitability for transdermal applications where flexibility and durability are crucial factors [44].

Measuring tensile strength

NP-3 patches were cut into standardized sizes and subjected to tensile strength testing using a tensiometer. The tensiometer measures the force required to break the patch, expressed as kg/cm^2, providing crucial insights into the mechanical strength and integrity of the patch material. This method evaluates the ability of NP-3 to withstand stretching forces, which is essential for assessing its durability and reliability in transdermal drug delivery applications [45].

Assessing water vapour transmission rate (WVT)

The WVT rate, which indicates the moisture permeability of NP-3, is determined using glass vials containing anhydrous fused calcium chloride. NP-3 patches are affixed securely over the vials, and the initial weights are recorded. These assemblies are then exposed to a specific relative humidity environment for 24 h. After exposure, the patches are reweighed to measure the weight change due to moisture transmission through the patches [46]. This method allows for the quantification of NP-3's ability to resist or facilitate moisture passage, providing critical data on its suitability for transdermal applications where moisture control is essential for drug stability and effectiveness.

***In vitro* drug permeation (DP) studies**

For in vitro DP studies, a Modified Franz diffusion cell setup was employed, featuring a blended cellulose ester membrane that was pre-soaked in distilled water overnight. Transdermal patches were securely affixed to the dialysis membrane and placed in the donor compartment of the diffusion cell. The receptor compartment contained 85 ml of pH 7.4 Phosphate-Buffered Saline (PBS) maintained at 37±2 °C, with stirring at 500 rpm to facilitate permeation. Sampling occurred at precise intervals over 24 h under sink conditions, ensuring a constant concentration gradient. Samples collected from the receptor compartment were analyzed at 237 nm using a UV-visible spectrophotometer to quantify drug permeation [47]. This setup allowed for the assessment of NP-3's ability to deliver drugs across the skin barrier, providing crucial data on its potential effectiveness in therapeutic applications [48, 49].

***Ex vivo* skin DP studies**

In this study, goat skin obtained from a local market was meticulously cleaned using water and a scalpel to remove

impurities. Subsequently, the cleaned skin was immersed in an isotonic solution for 1 h to maintain hydration and simulate physiological conditions. Mounted onto a Modified Franz diffusion cell setup, transdermal patches were applied to the skin and securely affixed to the donor compartment. The receptor compartment contained 85 ml of pH 7.4 PBS at 37±2 °C, stirred at 500 rpm to ensure uniform conditions for permeation studies over 24 h. Sampling was conducted at specific intervals to monitor drug permeation through the skin, and samples from the receptor compartment were analyzed at 237 nm using a UV-visible spectrophotometer, mirroring the procedures of earlier in vitro studies [50]. This experimental approach provided insights into how NP-3 interacts with goat skin under physiological conditions, crucial for assessing its potential effectiveness in transdermal drug delivery applications [51, 52].

NSD discharge kinetics study

Data obtained from both *in vitro* and *ex vivo* DP studies are analyzed by fitting them to various mathematical kinetic models. These models are instrumental in elucidating the mechanisms and patterns of NSD discharge from transdermal NP-3 patches. By studying these discharge kinetics, researchers can gain insights into how the drug is discharged over time, which is crucial for designing and optimizing drug delivery systems [53, 54]. This approach allows for the refinement of NP-3 formulations to achieve desired drug discharge profiles, enhancing their efficacy and suitability for therapeutic applications [55, 56].

Skin irritation study

The experimental procedures were ethically approved by the Institutional Animal Ethical Committee (IAEC No. 1519/PO/Re/S/11/CCSEA). All experiments were conducted in accordance with the guidelines and regulations for the care and use of laboratory animals as set forth by the Committee for the Purpose of Control and Supervision of Experiments on Animals (CPCSEA). Efforts were made to minimize animal suffering and reduce the number of animals used. The animals were obtained from the animal facility at Santhiram College of Pharmacy, Nandyal, and were housed in standard laboratory conditions with a 12 h light/dark cycle, temperature of 22±2 °C, and humidity of 50±5%. Rabbits are acclimated for at least 7 days before the start of the experiment. Provide a standard diet and water ad libitum. The health status of the animals was monitored regularly, and only healthy animals with no prior exposure to the test compound were included in the study. To assess skin irritation, the patch was uniformly spread over an 8.70 cm^2 area of the skin. The skin surface was then observed for visible changes such as erythema at 24, 48, and 72 h post-application of the patch. Erythema scores were assigned on a scale of 0 to 4 based on the severity of redness [57, 58].

Comparison of permeation with normal patch

For comparing DP between the optimized NP-3 and normal TPs, the procedure followed the methodology described earlier for in vitro DP studies. This included using a modified Franz diffusion cell setup where the patches were affixed to a dialysis membrane, ensuring consistent conditions such as temperature and stirring speed. Samples were collected at specific intervals, with phosphate buffer replenished to maintain sink conditions conducive to drug discharge. Drug content analysis in the collected samples was performed using a UV-visible spectrophotometer [59]. This standardized approach facilitated a rigorous comparison of DP characteristics between NP-3 and conventional transdermal patches, offering valuable insights into the performance and effectiveness of the optimized NP-3 [60, 61].

Statistical analysis

The results were presented as mean±standard deviation, with a sample size of n = 3. Simple regression analysis was conducted using GraphPad Prism 7 software to explore potential relationships or trends within the dataset. This statistical approach enabled the interpretation of experimental findings and the assessment of any observed associations between variables.

Accelerated stability studies

The optimized formulation (NP-3) was stored at accelerated testing conditions (40±2.2 °C and 75±5.2% RH) for three months. For these studies, the films were wrapped in aluminum foil and placed in an environmental chamber. Samples were withdrawn at regular times. The films were then evaluated for physicochemical properties [62].

RESULTS AND DISCUSSION

Compatibility studies

DSC thermograms of NSD alone and in combination with excipients were utilized to illustrate the effective interaction of the NSD with the excipients. These thermograms indicate good miscibility between the NSD and the excipients, demonstrating their compatibility and suggesting potential enhancements in formulation stability and effectiveness (fig. 1).

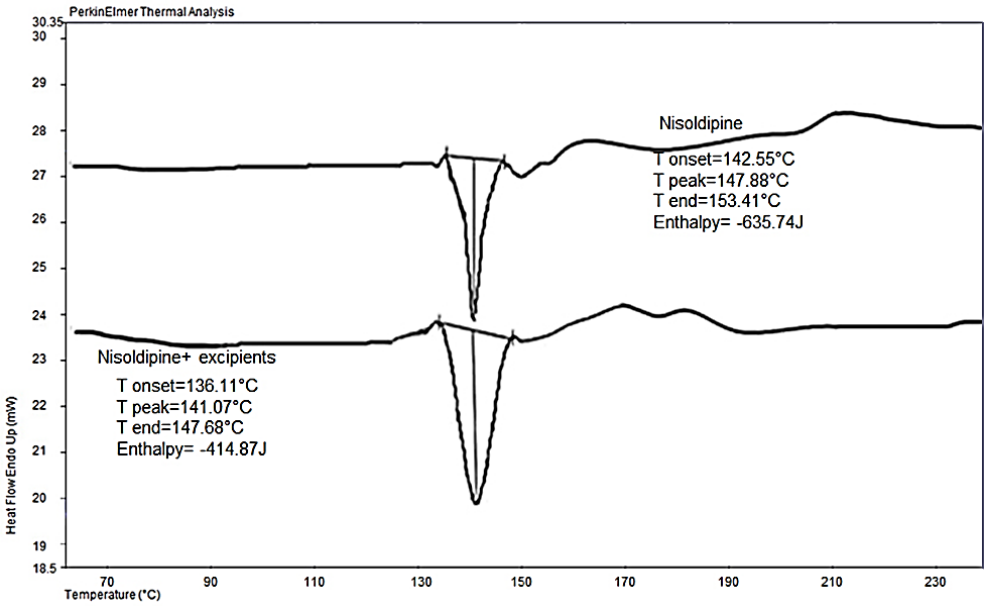

Fig. 1: DSC thermograms of NSD alone and its combinations with excipients

The characteristic peaks and stretches observed in the FTIR of the NSD remained undisturbed even when combined with the excipients used. This observation indicates that the chemical bonds and functional groups of the NSD were retained without alteration or significant interaction with the excipients. Such stability in the FTIR spectrum suggests that the NSD and excipients are compatible, supporting their potential application together in formulations without compromising the integrity of the NSD's chemical structure (fig. 2 and 3).

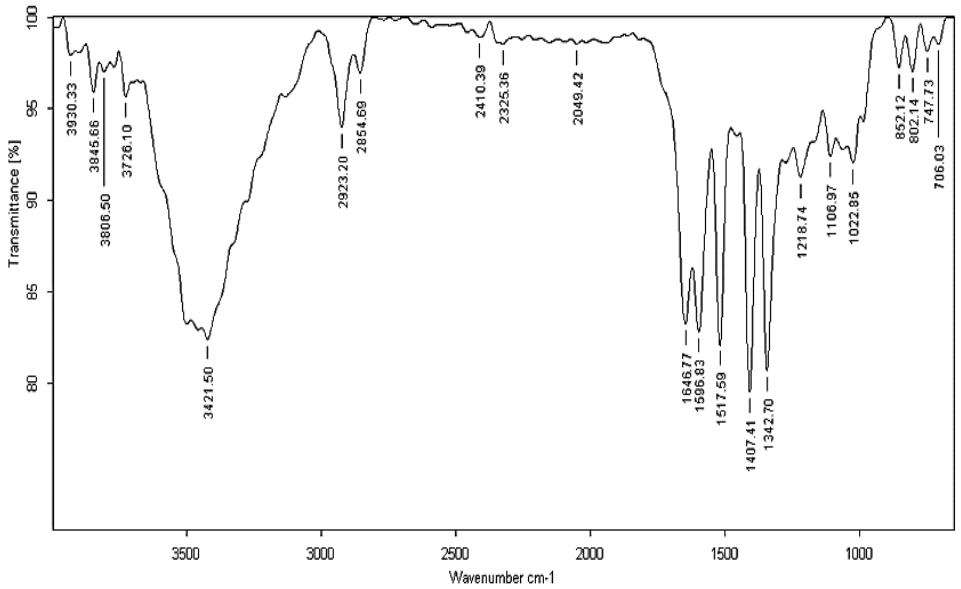

Fig. 2: FTIR spectrum of NSD pure

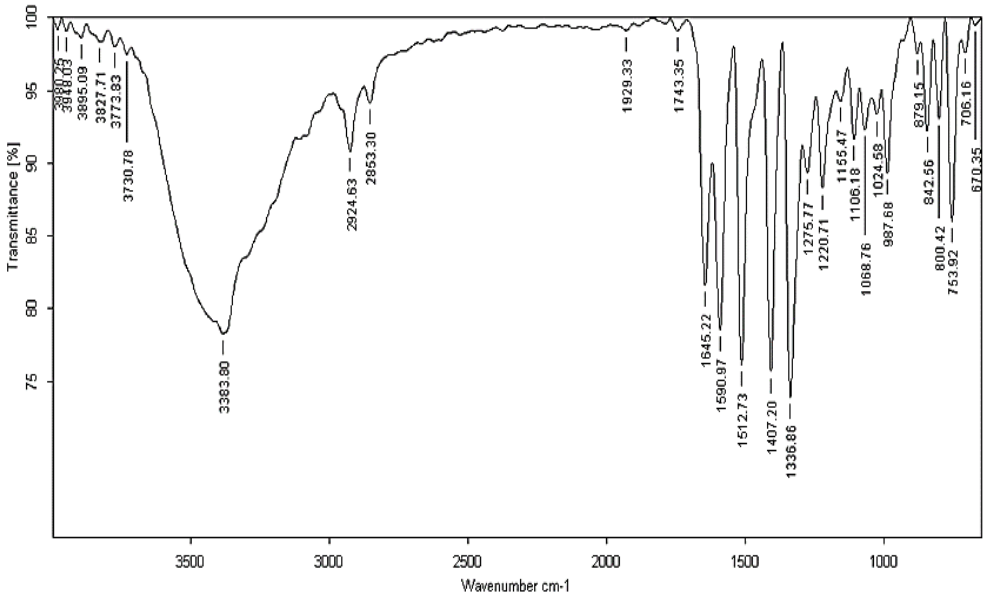

Fig. 3: FTIR spectrum of NSD with polymers

The PDI of the NT, as depicted in fig. 4, offers critical insights into the uniformity of particle sizes within the NTs. A PDI value close to zero indicates a narrow size distribution, with particles predominantly of similar sizes. Conversely, a higher PDI suggests a broader range of particle sizes, indicating greater variability within the NTs [63]. This characterization is pivotal for assessing the consistency and quality of NT formulations, guiding further optimization efforts to achieve desired particle size uniformity for enhanced drug delivery performance.

Deformability

The VS of NT before and after extrusion serves as a critical indicator of their deformability, which reflects the flexibility of these lipid-based nanoparticles. Initially, NT typically exhibits a range of sizes with some variability in diameter due to diverse lipid compositions and assembly processes. However, after extrusion, NT undergoes a process of size reduction and homogenization, resulting in a more uniform and smaller size distribution. This reduction in VS indicates enhanced deformability, as the NT can more easily adapt to changes in their environment and traverse biological barriers such as the skin's stratum corneum. Therefore, comparing VS before and after extrusion provides valuable insights into the deformability and flexibility of NT, essential characteristics for effectively delivering NSD across various applications [64]. This property enhances their potential for optimized drug delivery systems capable of overcoming barriers and improving therapeutic outcomes (table 2).

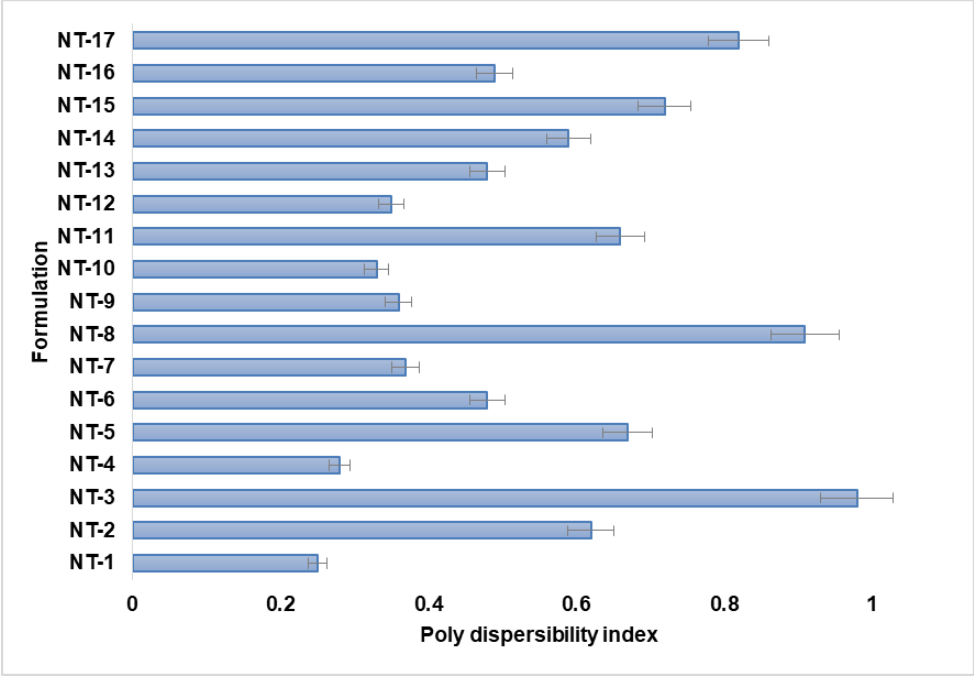

Fig. 4: Poly dispersibility index of the formulations, value are given in mean±SD; n=3. Error bars indicate SD

Table 2: Vesicle size of NT before and after extrusion representing their deformability

Trials	Before extrusion (nm)	After extrusion (nm)	Deformability index	Zeta potential (mV)
NT-1	333±2.3.6	312±3.48	6.31±0.23	-21
NT-2	360±3.62	341±5.25	5.28±0.27	-29
NT-3	218±5.25	202±3.84	7.34±0.22	-48
NT-4	256±6.22	239±2.64	6.64±0.14	-20
NT-5	275±0.92	256±2.61	6.91±0.03	-30
NT-6	384±1.05	372±1.90	3.12±0.07	-23
NT-7	305±1.65	289±3.95	5.24±0.06	-32
NT-8	361±2.84	345±2.38	4.43±0.07	-25
NT-9	396±3.85	375±4.15	5.30±0.08	-22
NT-10	265±4.82	249±5.65	6.04±0.05	-40
NT-11	251±7.26	241±4.08	3.98±0.02	-30
NT-12	385±6.62	366±2.18	4.93±0.07	-27
NT-13	230±5.15	220±6.33	4.35±0.08	-35
NT-14	221±2.08	211±5.92	4.52±0.06	-41
NT-15	241±1.45	226±4.82	6.22±0.07	-36
NT-16	219±4.62	209±3.65	4.57±0.04	-38
NT-17	254±2.68	237±0.28	6.69±0.03	-37

NT: Nisoldipine transferosomes, value are given in mean±SD; n=3.

Confocal laser scanning microscopy

CLSM was employed to assess the depth of NSD penetration through vesicles in developed NT. CLSM images depicted a well-distributed presence of NT throughout the skin layers, characterized by high fluorescence intensity. Specifically, the CLSM image of optimized NT loaded with Rhodamine B dye exhibited significantly deeper penetration and higher fluorescence intensity compared to Rhodamine B dye solution alone. This enhanced penetration and fusion with membrane lipids in the deeper skin layers highlight the NT's effectiveness in delivering the NSD. These findings align with previous research, affirming the potential of NT to facilitate improved NSD penetration into the skin compared to plain dye solutions, thus enhancing their therapeutic application capabilities (fig. 5). CLSM is a powerful imaging technique used to explore the depth of penetration and distribution of NSDs within biological tissues. In our study, CLSM was employed to evaluate the performance of a developed NT for delivering the NSD. The CLSM images provided crucial insights into the distribution of the NT within the skin layers. The results illustrated the effective distribution of NT throughout the skin layers, evident from the high fluorescence intensity observed in the CLSM images. Specifically, the optimized NT loaded with Rhodamine B dye exhibited significantly deeper penetration and higher fluorescence intensity compared to Rhodamine B dye solution alone. This excellent Ultra deformable liposome transport of Rhodamine B demonstrates that it enhanced penetration and then merged with the membrane lipids in the deeper layers of the skin, validating the findings of earlier studies [65]. This enhanced penetration is attributed to NT's efficient delivery of the NSD into deeper skin layers. Additionally, the observed fusion of NT with membrane lipids in the deeper skin layers indicates its potential to facilitate NSD delivery through interactions with the skin's lipid barrier [66]. These findings align with previous research, confirming the efficacy of NT in enhancing drug permeation and delivery capabilities.

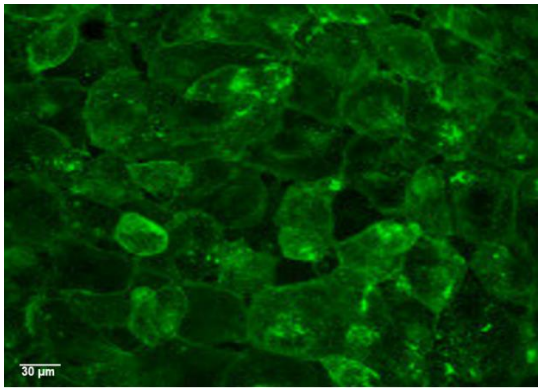

Fig. 5: Confocal laser scanning microscopy pictures of the optimized formulations of nisoldipine transferosomes-3

Results of the effect of independent variables on VS, EE, and ZP

The characterization of transferosomes revealed vesicle sizes ranging from 124±2.25 to 400±1.55 nm, EE % from 52.88±0.23 to 90.01±1.58%, and ZP between-48 to-20 mV. The broad vesicle size range suggests variations in the formulation process, such as sonication time and lipid concentration, which could impact the uniformity of vesicle sizes. Smaller vesicles may enhance cellular uptake, while larger ones can facilitate sustained release. The high EE%, reaching up to 90.01±1.58%, indicates effective encapsulation of active pharmaceutical ingredients, though the lower end (52.88±0.23%) points to potential suboptimal conditions in some formulations (fig. 6). Optimizing the lipid-to-drug ratio and preparation techniques could improve EE% consistency. The negative ZP values signify good colloidal stability, as high absolute values prevent particle aggregation. Ensuring these ZP ranges is crucial for the long-term stability of the transferosomes [67]. Overall, the transferosomes exhibit promising characteristics for drug delivery systems, with further optimization needed to achieve consistent and desirable properties.

Effect sizes

For each outcome measure, the effect size was calculated to provide additional context to the statistical significance. Effect sizes were reported as Cohen's d for comparing two groups and partial eta squared (η^2) for ANOVA.

Vesicle size

The mean VS for the optimized NT-3 was 150 nm (SD = 19.91 nm). The effect size for the difference in vesicle size between NT-3 and the control formulation was large (Cohen's d = 1.25), indicating a substantial difference. Image shown in fig. 7A. The ZP image is shown in fig. 7B. SEM micrograph of optimized formulation (NT-3) is shown in fig. 7C.

Entrapment efficiency

The EE% for NT-3 was 90.01% (SD = 1.58%). The effect size for the difference in EE% between NT-3 and the control was also large (Cohen's d = 1.30).

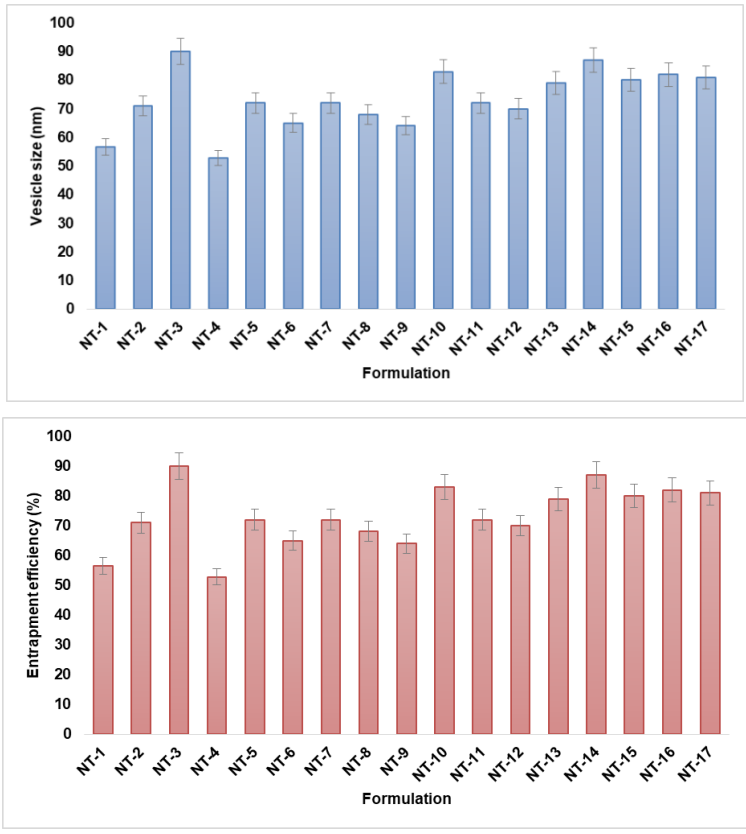

Fig. 6: Vesicular size and entrapment efficiency of the vesicles, values are given in mean±SD; n=3. Error bars indicate SD

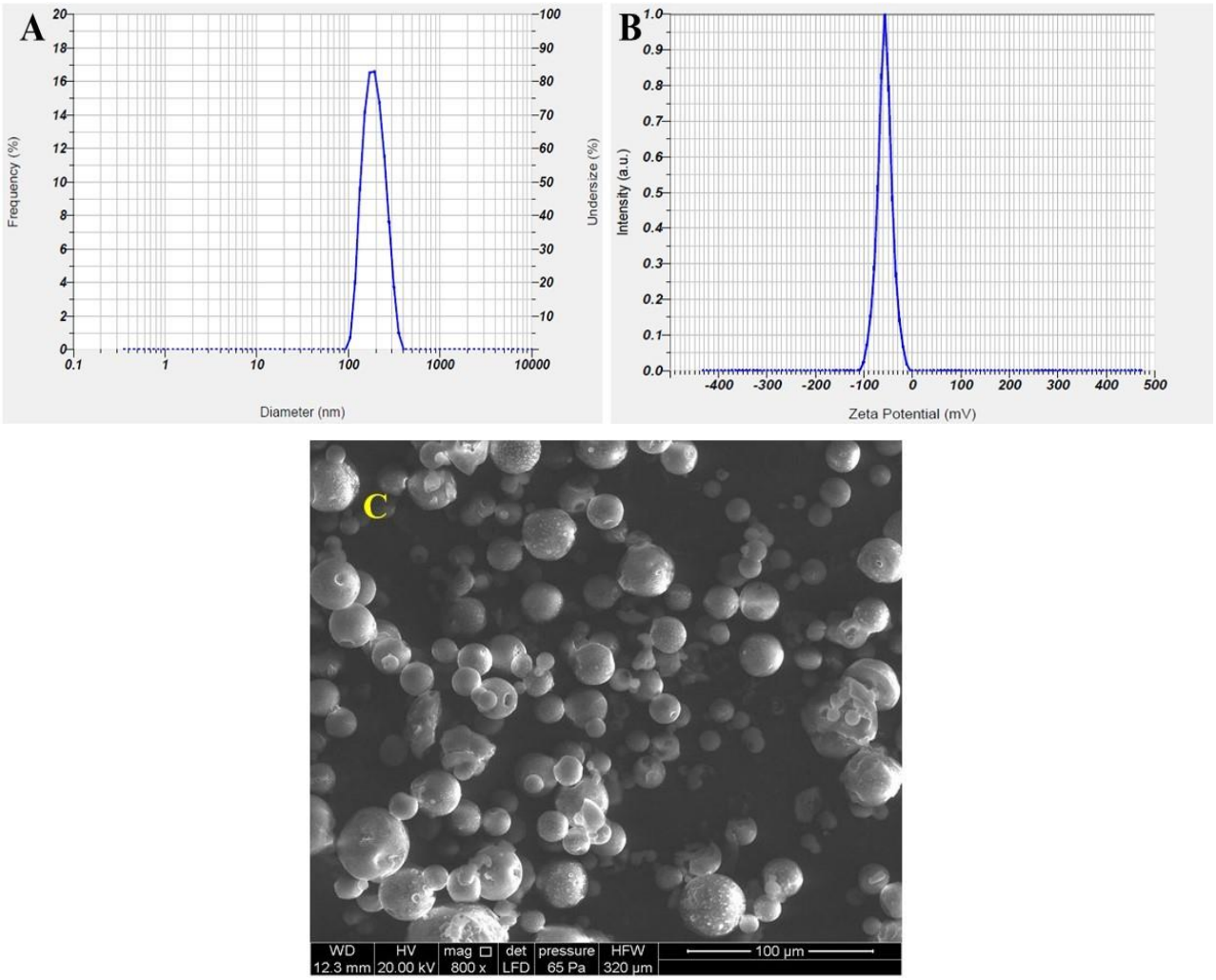

Fig. 7: Images showing (A) Vesicle size and vesicle size distribution, (B) Zeta potential (C) SEM micrograph of optimized formulation of nisoldipine transferosomes-3

The model F-value of 35.45 suggests that the model is highly significant, with only a 0.01% chance that such a large F-value could occur due to noise, indicating strong support for the model's validity. Significant model terms, including A, B, AB, AC, BC, A^2, B^2, and C^2, have p-values<0.05, further reinforcing their importance in the model. The Lack of Fit F-value of 0.88 indicates that the Lack of Fit is not significant relative to the pure error, with a 52.12% chance that such a value could occur due to noise. This lack of significance is favorable, indicating that the model fits well and can effectively capture the underlying relationships. Both the predicted R^2 of 0.8429 and the adjusted R^2 of 0.9509 are in reasonable agreement, differing by<0.2. This suggests that the model's predictive power is consistent across different datasets, further bolstering its reliability.

Adeq. Precision, with a ratio of 17.71, well above the desirable threshold of 4, the model demonstrates an adequate signal-to-noise ratio, indicating that it can effectively navigate the design space and provide valuable insights.

The model F-value of 19.41 specifies significance, with only a 0.01% probability that such a large F-value could occur due to noise. This suggests strong support for the model's validity. Significant model terms, including A, B, AB, BC, A^2, B^2, and C^2, have p-values<0.05, indicating their importance in the model.

The Lack of Fit F-value of 0.89 suggests that the Lack of Fit is not significant relative to the pure error, with a 52.01% chance that such a value could occur due to noise. This lack of significance is favorable, indicating a good fit for the model. Both the predicted R^2 of 07176 and the adjusted R^2 of 0.9119 show reasonable agreement, with a difference of<0.2, suggesting the model's predictive power is reliable across different datasets. Adeq. Precision, which measures the signal-to-noise ratio, is crucial for assessing model performance. With a ratio of 14.69, well above the desirable threshold of 4, the model demonstrates an adequate signal-to-noise ratio. This indicates that the model can effectively navigate the design space and provide meaningful insights.

The model F-value of 20.65 specifies significance, with only a 0.01% probability that such a large F-value could occur due to noise. This suggests strong support for the model's validity. Significant model terms, including A, B, AB, BC, A^2, B^2, and C^2, have p-values<0.05, indicating their importance in the model.

The Lack of Fit F-value of 0.99 suggests that the Lack of Fit is not significant relative to the pure error, with a 48.22% chance that such a value could occur due to noise. This lack of significance is favorable, indicating a good fit for the model. Both the predicted R^2 of 0.7199 and the adjusted R^2 of 0.9170 show reasonable agreement, with a difference of<0.2, suggesting the model's predictive power is reliable across different datasets. Adeq. Precision, which measures the signal-to-noise ratio, is crucial for assessing model performance. With a ratio of 15.03, well above the desirable threshold of 4, the model demonstrates an adequate signal-to-noise ratio. This indicates that the model can effectively navigate the design space and provide meaningful insights (tables 3 and 4).

Table 3: ANOVA for the responses assessed

Source	Sum of squares	F-value	p-value	
ANOVA for VS				
Model	1.266	35.45	<0.0001	Significant
A-DPPC	27848.00	70.19	<0.0001	
B-Span-80	3403.13	8.58	0.0221	
C-stirring speed	3081.13	7.77	0.0270	
AB	17161.00	43.25	0.0003	
AC	2500.00	6.30	0.0404	
BC	37442.25	94.37	<0.0001	
A^2	2300.59	5.80	0.0469	
B^2	17857.96	45.01	0.0003	
C^2	11883.22	29.95	0.0009	
ANOVA for EE				
Model	1612.25	19.41	0.0004	Significant
A-DPPC	142.80	15.47	0.0057	
B-Span-80	129.61	14.04	0.0072	
C-stirring speed	0.5000	0.0542	0.8226	
AB	665.64	72.12	<0.0001	
AC	2.25	0.2438	0.6366	
BC	110.25	11.94	0.0106	
A^2	311.41	33.74	0.0007	
B^2	132.04	14.31	0.0069	
C^2	65.69	7.12	0.0321	
ANOVA for ZP				
Model	981.17	20.65	0.0003	Significant
A-DPPC	144.50	27.37	0.0012	
B-Span-80	136.13	25.79	0.0014	
C-stirring speed	0.1250	0.0237	0.8820	
AB	324.00	61.38	0.0001	
AC	0.0000	0.0000	1.0000	
BC	110.25	20.89	0.0026	
A^2	108.44	20.54	0.0027	
B^2	33.60	6.37	0.0396	
C^2	98.02	18.57	0.0035	

Table 4: The results of regression analysis for Y_1, Y_2, and Y_3 for fitting to the quadratic model

Response	r^2	Adjusted r^2	Predicted r^2	SD	%CV	Adequate precision
Y_1	0.9785	0.9509	0.8429	19.92	8.95	17.71
Y_2	0.9615	0.9119	0.7176	3.04	4.15	14.69
Y_3	0.9637	0.9170	0.7199	2.30	7.31	15.03
Equation						
Y_1=+156+59.0A+20.62B+19.62C+65.5AB+25AC+96.75BC+23.38A^2+65.13B^2+53.13C^2						
Y_2=+81.8-4.22A+4.03B-0.25C-12.9AB+0.75AC-5.25BC-8.6A^2-5.6B^2-3.95C^2						
Y_3=-37.4+4.25A-4.13B+0.125C+9.0AB+0.00AC+5.25BC+5.08A^2+2.83B^2+4.82C^2						

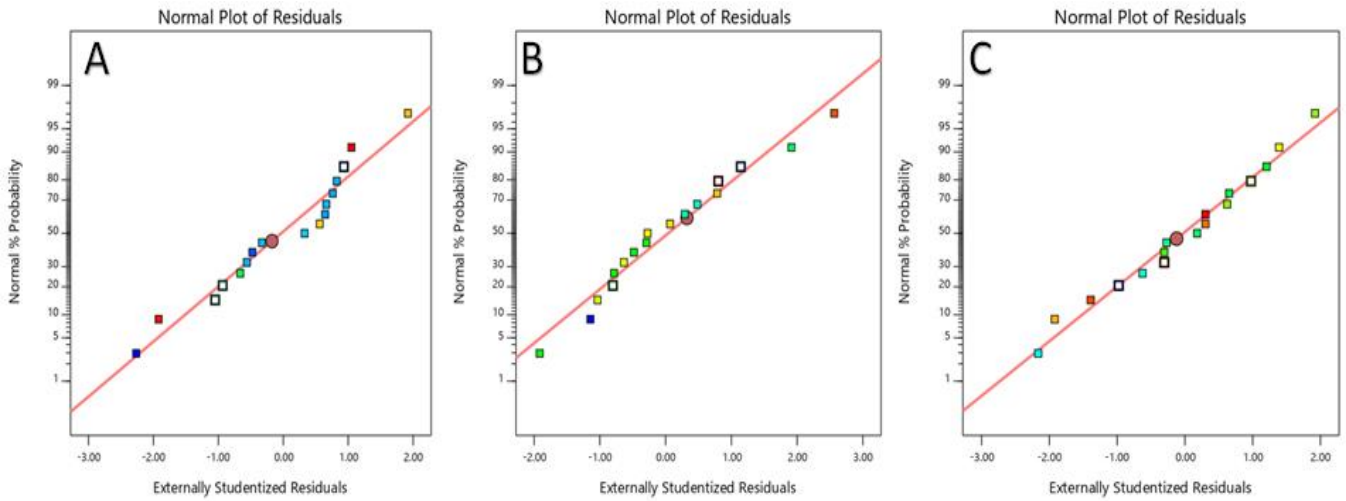

Fig. 8: Normal plot of residuals for the responses: A) Vesicular size, B) Entrapment efficiency, and C) Zeta potential, residuals vs. predicted for the responses

The normal plot of residuals for the responses (fig. 8A, B, and C) evaluates whether the residuals follow a normal distribution, a key assumption in statistical analysis. If the residuals are normally distributed, the points will lie on a straight line; deviations indicate potential issues with this assumption. Residuals vs. predicted plots illustrate the relationship between observed residuals and predicted values, helping to identify patterns or trends. Ideally, residuals should be randomly scattered around zero; patterns suggest model inadequacies like non-linearity or heteroscedasticity. Cook's distance plots measure each observation's influence on the model's parameters. High Cook's distances indicate observations with substantial impact, possibly pointing to influential data points or outliers that require further investigation. Together, these diagnostic tools ensure model assumptions are met, identify areas for improvement, and confirm the reliability of the study's results.

The contour plots for responses in fig. 9A (VS), 9B (EE), and 9C (ZP) depict the relationship between the independent variables and the corresponding response variables. These plots illustrate how changes in the levels of the independent variables affect the values of the response variables, providing insights into the optimal conditions for achieving desired outcomes. Additionally, the 3D plots for responses in fig. 9D (VS), 9E (EE), and 9F (ZP) offer a visual representation of the interaction between multiple IVs and their impact on the response variables [68]. These plots enable a more comprehensive understanding of the relationships between the variables, facilitating the identification of optimal parameter settings for maximizing VS, EE, and ZP.

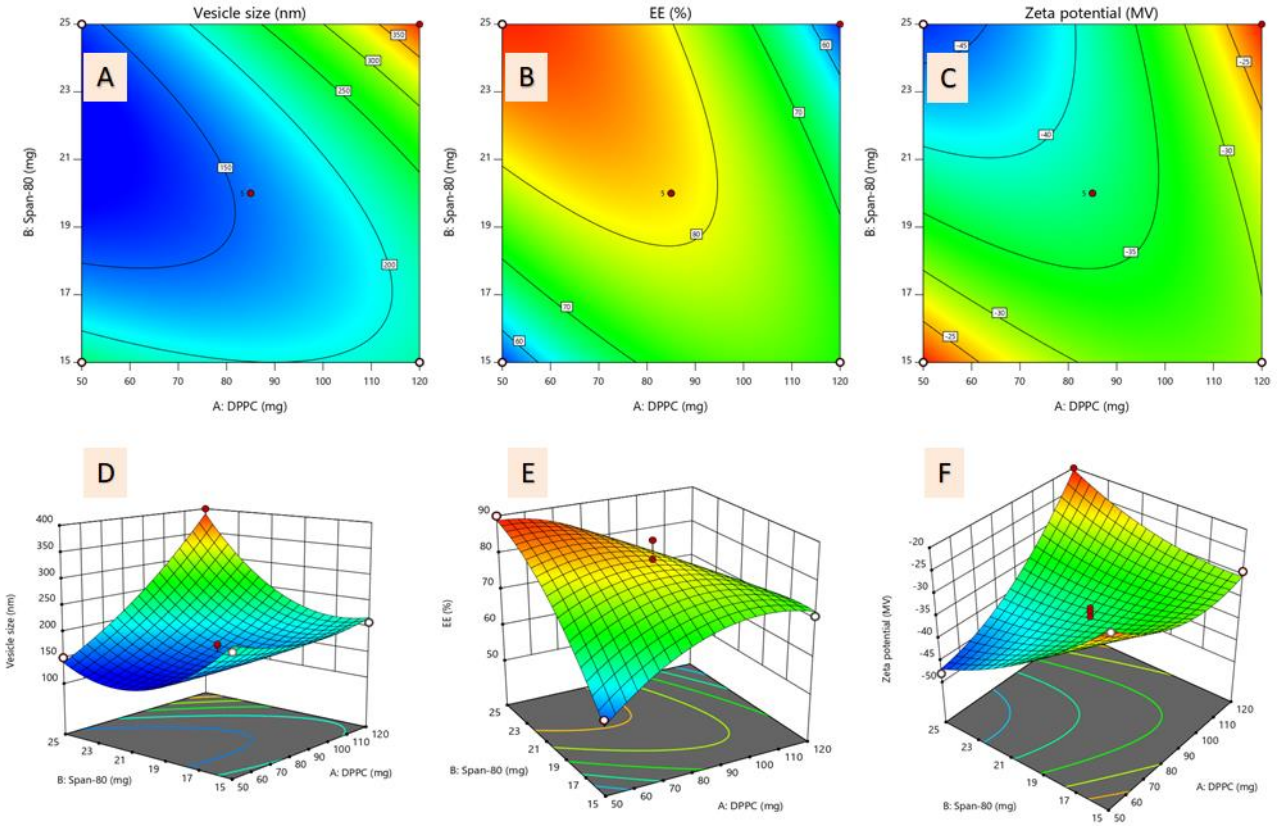

Fig. 9: Contour plots for the responses: A) Vesicular size, B) Entrapment efficiency, and C) Zeta potential. 3D plots for the responses: D) Vesicular size, E) Entrapment efficiency, and F) Zeta potential

Among the NTs, formulation NT-3 demonstrated smaller VS, improved ZP, and higher EE%. Consequently, this formulation was further incorporated into TPs.

Evaluation results of NP-3

The uniformity in patch thickness was 0.66±0.02 mm, underscoring consistent manufacturing processes. Similarly, the weight per square inch was 382.1±1.69 mg, further demonstrating formulation uniformity. The minimal WVT Rate (1.54±0.01 g/m^2/24h) and low moisture content (1.07±0.01%) indicate excellent moisture barrier properties. Additionally, moisture uptake within acceptable limits (3.78±0.01%) reflects stability under varying environmental conditions [69]. Moreover, the uniform NSD content and good tensile strength exceeding 2.56±0.02 kg/cm^2 ensure consistent dosage delivery and mechanical integrity of NP-3. These comprehensive quality assessments highlight the reliability and robustness of NP-3 for potential pharmaceutical applications.

Results of FE and NSD permeation

These findings indicate that the NP-3 formulation exhibits favorable flexibility, a crucial characteristic for transdermal delivery systems, with an FE of 97.67±0.47. This data underscores the efficacy of the TPs in facilitating DP of 86.39±2.64% within a relatively short timeframe. Overall, these results suggest that the NP-3 formulation holds promise for efficient drug delivery through the skin barrier, offering potential advantages in terms of patient convenience and therapeutic efficacy [70]. Furthermore, the results reveal that the NP-3 formulation exhibits favorable release characteristics over an extended period. Together, these findings suggest that the NP-3 formulation demonstrates promising performance not only in terms of sustained discharge but also in permeating through biological skin barriers, indicating its potential efficacy for transdermal drug delivery applications.

NSD release kinetics results

The kinetics of NSD discharge from the dosage form demonstrated adherence to the Korsmeyer-Peppas model (R^2 = 0.9957), indicating a non-Fickian release pattern (n = 0.6548). This finding suggests that the discharge of NSD from the NP-3 is not solely governed by simple diffusion processes but also involves additional mechanisms such as swelling and erosion of the polymer matrix. The Korsmeyer-Peppas model is commonly used to describe NSD discharge from polymeric

systems, offering insights into the discharge mechanisms and enabling the prediction of release profiles over time [71]. The identification of a non-Fickian release pattern implies a complex interplay of factors influencing NSD release kinetics, highlighting the importance of further understanding the NP-3's behavior to optimize NSD delivery strategies.

Results of the skin irritation study for the optimized patch along with comparison with a normal TPs

The study evaluating NP-3 on rabbit skin for signs of erythema provides valuable insights into its safety and suitability. Using a scale from 0 to 4 to assess erythema severity, the study consistently found no indications of erythema or oedema throughout the application period, demonstrating excellent tolerance of NP-3 by rabbit skin. This is particularly significant given that rabbit skin shares similarities with human skin, suggesting the potential relevance of these findings to human applications. Statistical averaging of scores enhances reliability, accommodating individual variations among the rabbits. Overall, these results indicate a promising safety profile for NP-3, highlighting its potential for clinical use.

Fig. 10 illustrates the comparison between an optimized patch (NP-3) and a conventional TP containing the same drug (NP-N). Contrasting the NSD normal patch (NP-N) with NP-3 reveals significant differences in drug release kinetics and resulting plasma concentrations. NP-3 demonstrates prolonged drug discharge profiles, indicating controlled release over time compared to the relatively rapid discharge observed with NP-N. As a result, NP-3 achieves higher drug plasma concentrations.

The extended drug discharge observed with transferosomes can be attributed to their unique structure, which allows for NSD encapsulation within vesicles. This encapsulation enables controlled discharge and enhances drug bioavailability, highlighting transferosomes as a promising drug delivery system for improving therapeutic outcomes [72].

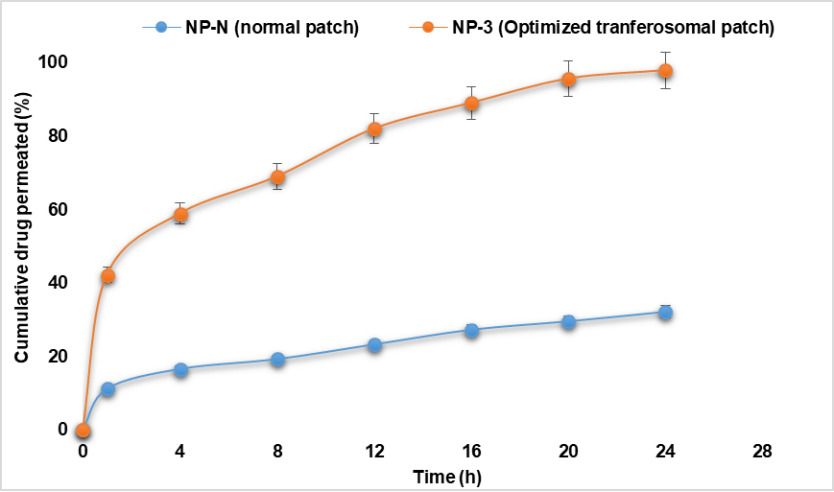

Fig. 10: Comparision of optimized transferosomal patch (NP-3) with the normal patch; values are given in mean±SD; n=3. Error bars indicate SD

Table 5: Physical assets of the optimized transferosomal patch (NP-3) during stability studies

Optimized batch	Sampled time	Parameters assessed					
NP-3		Moisture content (%)	Tensile strength (kg/cm²)	Drug permeated at 24h (%)	Weight per square inch (mg)	Water vapour transition rate (g/m²/d)	Folding endurance
	Day 1	3.78±0.01	2.56±0.02	86.39±2.64	382±11.69	1.54±0.01	97.67±0.47
	30th d	3.77±0.01	2.58±0.02	86.24±1.37	381±10.27	1.53±0.02	96.34±0.47
	60th d	3.78±0.01	2.55±0.02	86.16±1.33	380±12.82	1.55±0.01	95.00±0.82
	90th d	3.79±0.01	2.54±0.01	86.22±3.65	381±10.17	1.55±0.02	94.33±0.47

Value are given in mean±SD; n=3.

Results of stability studies

The films were analyzed at 0 days and at 1, 2, and 3-month intervals for physical assets, revealing that the NP-3 retained the specifications even after the stressed storage conditions (table 5).

CONCLUSION

The study effectively addressed the challenges associated with oral delivery of NSD by developing transferosomal transdermal patches. Utilizing a comprehensive methodology involving NSD encapsulation within transferosomes and subsequent integration into TPs using DPPC, span-80, and cholesterol. The study achieved notable enhancements in NSD permeation and efficacy. The optimized NP-3 exhibited favorable physicochemical properties, enhanced NSD permeation in both *in vitro* and *ex-vivo* studies, and demonstrated minimal skin irritation. The NP-3 composition displays good FE 97.67±0.47, required for transdermal systems, and successfully allows DP at 86.39±2.64% in a short timescale. Importantly, these formulations displayed prolonged NSD discharge profiles compared to conventional NSD patches. These findings indicate that NP-3 represent a promising approach for effective transdermal delivery, potentially offering sustained and controlled management of hypertension. This advancement holds significant promise for improving patient adherence and therapeutic outcomes in hypertension treatment.

FUNDING

Nil

AUTHORS CONTRIBUTIONS

Mothilal. M contributed to the study design, while D. Maheswara Reddy collaborated with data collecting, analysis, and paper writing, assuring a collaborative and balanced effort throughout the research

process. Both writers reviewed and approved the final draft.

CONFLICT OF INTERESTS

All authors declare no conflict of interest

REFERENCES

1. Godfraind T. Discovery and development of calcium channel blockers. Front Pharmacol. 2017 May 29;8:286. doi: 10.3389/fphar.2017.00286, PMID 28611661.
2. Dens JA, Desmet WJ, Coussement P, DE Scheerder IK, Kostopoulos K, Kerdsinchai P. Long term effects of nisoldipine on the progression of coronary atherosclerosis and the occurrence of clinical events: the NICOLE study. Heart. 2003;89(8):887-92. doi: 10.1136/heart.89.8.887, PMID 12860866.
3. Preeti SS, Sambhakar S, Malik R, Bhatia S, Harrasi AA, Saharan R. Lipid horizons: recent advances and future prospects in LBDDS for oral administration of antihypertensive agents. Int J Hypertens. 2024;2024(1):2430147. doi: 10.1155/2024/2430147, PMID 38410720.
4. Pepine CJ, Cooper DE Hoff RM, Weiss RJ, Koren M, Bittar N, Thadani U. Comparison of effects of nisoldipine extended-release and amlodipine in patients with systemic hypertension and chronic stable angina pectoris. Am J Cardiol. 2003;91(3):274-9. doi: 10.1016/s0002-9149(02)03154-5, PMID 12565082.
5. Dole R, Kothapally D, Chukkala S, Thatipelli RC. Approaches to improve oral bioavailability of antihypertensive drugs: a mini review. J Drug Delivery Ther. 2023;13(5):73-7. doi: 10.22270/jddt.v13i5.5814.
6. Chu PC, Liao MH, Liu MG, LI CZ, Lai PS. Key transdermal patch using cannabidiol-loaded nanocarriers with better pharmacokinetics *in vivo.* Int J Nanomedicine. 2024 May 16;19:4321-37. doi: 10.2147/IJN.S455032, PMID 38770103.
7. Fernandez Garcia R, Lalatsa A, Statts L, Bolas-Fernandez F, Ballesteros MP, Serrano DR. Transferosomes as nanocarriers for drugs across the skin: quality by design from lab to industrial scale. Int J Pharm. 2020 Jan 5;573:118817. doi: 10.1016/j.ijpharm.2019.118817, PMID 31678520.
8. Narvekar MN, Redkar MM, Bhosale MN. Self-assembled ultradeformable phospholipid vesicles with edge activators for delivery of transcutaneous bioactives. Indo Am J Pharm Res. 2019;9(12):543-52.
9. Kumar PK, Kumar RS. Review on transferosomes and transferosomal gels. J Pharm Res Int. 2021;33(43B):114-26. doi: 10.9734/jpri/2021/v33i43B32532.
10. Wang J, Zhao Y, Zhai B, Cheng J, Sun J, Zhang X. Phloretin transfersomes for transdermal delivery: design optimization and *in vivo* evaluation. Molecules. 2023;28(19):6790. doi: 10.3390/molecules28196790, PMID 37836633.
11. Jain AK, Kumar F. Transfersomes: ultradeformable vesicles for transdermal drug delivery. Asian J Biomater Res. 2017;3:1-3.
12. Rajkumar J, Sree Lakshmi RK, Vineesha S. A new approach to transdermal drug delivery using transfersomes based nano encapsulation: a research update. Asian J Pharm Res Dev. 2022;10(1):64-70. doi: 10.22270/ajprd.v10i1.1082.
13. Sun Y, Zhang Y, Liu X, Tingting Y, Shen L, YE D. The preparation of high minoxidil loaded transfersomes and its gel for effective topical treatment of alopecia. J Drug Deliv Sci Technol. 2023 Jun;84:104458. doi: 10.1016/j.jddst.2023.104458.
14. Shravani Y, Ahad HA, Haranath C, Gari Poojitha B, Rahamathulla S, Rupasree A. Past decade work done on cubosomes using factorial design: a fast track information for researchers. Int J Life Sci Pharm Res. 2021;11(1):124-35. doi: 10.22376/ijpbs/lpr.2021.11.1.P124-135.
15. Mundarinti SH, Ahad HA. Past decade attempts on gastro retentive microspheres using factorial design: comprehensive literature. Int J Pharm Phytopharm Res. 2021;11(2):24-30. doi: 10.51847/XqUtLso9HJ.
16. Priyanka NV, Neeraja P, Mangilal T, Kumar MR. Formulation and evaluation of gel loaded with microspheres of apremilast for transdermal delivery system. Asian J Pharm Clin Res. 2019;12(2):411-7. doi: 10.22159/ajpcr.2019.v12i2.29374.
17. Choudhury D, Dutta KN, Kalita R. A review on transdermal patches used as an anti-inflammatory agent. Asian J Pharm Clin Res. 2021;14(12):21-6. doi: 10.22159/ajpcr.2021.v14i12.43277.
18. Simrah HA, Hafeez A, Usmani SA, Izhar MP. Transfersome an ultra deformable lipid-based drug nanocarrier: an updated review with therapeutic applications. Naunyn Schmiedebergs Arch Pharmacol. 2024;397(2):639-73. doi: 10.1007/s00210-023-02670-8, PMID 37597094.
19. Qosimah D, Widyarti S, Beltran M, Rifa IM. Improved cellular immunity and increased insulin in streptozotosin-induced mice using ethanol coriander (Coriandrum sativum) extract. Res J Pharm Technol. 2021;14(7):3689-94. doi: 10.52711/0974-360X.2021.00638.
20. Fouziya B, Abdul Ahad H, Swamy Charan D, Sri Vidya J, Chandana Reddy U, Nandini Reddy P. Fabrication and evaluation of cefpodoxime proxetil niosomes. Asian J Pharm Technol. 2022;12(2):109-12. doi: 10.52711/2231-5713.2022.00018.
21. Todke P, Polaka S, Raval N, Gondaliya P, Tambe V, Maheshwari R. Transfersome embedded gel for dual mechanistic delivery of anti-psoriatic drugs to dermal lymphocytes. J Microencapsul. 2022;39(6):495-511. doi: 10.1080/02652048.2022.2116119, PMID 35993180.
22. Riccardi D, Baldino L, Reverchon E. Liposomes transfersomes and niosomes: production methods and their applications in the vaccinal field. J Transl Med. 2024;22(1):339. doi: 10.1186/s12967-024-05160-4, PMID 38594760.
23. Haranath C. Recent advances in lipid-based nanovesicles for transdermal drug delivery. J Med Pharm Allied Sci. 2022 Dec 31;11(6):5375-81. doi: 10.55522/jmpas.V11I6.4273.
24. Abd El-Alim SH, Kassem AA, Basha M, Salama A. Comparative study of liposomes ethosomes and transfersomes as carriers for enhancing the transdermal delivery of diflunisal: *in vitro* and *in vivo* evaluation. Int J Pharm. 2019 May 30;563:293-303. doi: 10.1016/j.ijpharm.2019.04.001, PMID 30951860.
25. Amos WB, White JG. How the confocal laser scanning microscope entered biological research. Biol Cell. 2003;95(6):335-42. doi: 10.1016/s0248-4900(03)00078-9, PMID 14519550.
26. Teng X, LI F, LU C. Visualization of materials using the confocal laser scanning microscopy technique. Chem Soc Rev. 2020;49(8):2408-25. doi: 10.1039/C8CS00061A.
27. Waheed A, Aqil M, Ahad A, Imam SS, Moolakkadath T, Iqbal Z. Improved bioavailability of raloxifene hydrochloride using limonene containing transdermal nano-sized vesicles. J Drug Deliv Sci Technol. 2019 Aug;52:468-76. doi: 10.1016/j.jddst.2019.05.019.
28. Balata GF, Faisal MM, Elghamry HA, Sabry SA. Preparation and characterization of ivabradine HCl transfersomes for enhanced transdermal delivery. J Drug Deliv Sci Technol. 2020 Dec;60:101921. doi: 10.1016/j.jddst.2020.101921.
29. Kumar Jyothika LS, Abdul Ahad H, Haranath C, Kousar S, Pal Gowd HD, Halima Sadiya S. Types of transdermal drug delivery systems: a literature report of the past decade. RJPDFT. 2022;14(2):157-62. doi: 10.52711/0975-4377.2022.00025.
30. Mehra V, Pai A, B Bhat B, Ram HNA, Kamath BV. Prospective potential of enzymes from novel bacillus sonorensis: insights into the structural aspects industrial and therapeutic significance. Res J Pharm Technol. 2023;16(10):4671-6. doi: 10.52711/0974-360X.2023.00759.
31. Sarmah PJ, Kalita B, Sharma AK. Transfersomes based transdermal drug delivery: an overview. IJAPR. 2013;4(12):2555-63.
32. Babu GN, Muthukarupan M, Ahad HA. Neem fruit mucilage impact on acyclovir release at different intervals: a central composite design screening. Int J Pharm Res Allied Sci. 2021;10(4):131-41. doi: 10.51847/Uh1ekmZM0d.
33. Wong WF, Ang KP, Sethi G, Looi CY. Recent advancement of medical patch for transdermal drug delivery. Medicina (Kaunas). 2023;59(4):778. doi: 10.3390/medicina59040778, PMID 37109736.
34. Yilmaz EG, Ece E, Erdem O, Es I, Inci F. A sustainable solution to skin diseases: ecofriendly transdermal patches. Pharmaceutics. 2023;15(2):579. doi: 10.3390/pharmaceutics15020579, PMID 36839902.

35. Chaurasiya P, Ganju E, Upmanyu N, Ray SK, Jain P. Transfersomes: a novel technique for transdermal drug delivery. J Drug Delivery Ther. 2019;9(1):279-85. doi: 10.22270/jddt.v9i1.2198.
36. Ghosh S, Basak A. Design fabrication *in-vitro* and ex-vivo permeation study nisoldipine (nsp) loaded slns by modified solvent diffusion method. Res J Pharm Technol. 2024;17(5):2327-38. doi: 10.52711/0974-360X.2024.00365.
37. Islam N, Irfan M, Zahoor AF, Iqbal MS, Syed HK, Khan IU. Improved bioavailability of ebastine through development of transfersomal oral films. Pharmaceutics. 2021;13(8):1315. doi: 10.3390/pharmaceutics13081315, PMID 34452276.
38. Ahad A, Al Jenoobi FI, Al Mohizea AM, Aqil M, Kohli K. Transdermal delivery of calcium channel blockers for hypertension. Expert Opin Drug Deliv. 2013;10(8):1137-53. doi: 10.1517/17425247.2013.783562, PMID 23527660.
39. Pandit AP, Omase SB, Mute VM. A chitosan film containing quercetin loaded transfersomes for treatment of secondary osteoporosis. Drug Deliv Transl Res. 2020;10(5):1495-506. doi: 10.1007/s13346-020-00708-5, PMID 31942700.
40. Naji GH, Al Gawhari FJ. Evaluation of types and concentration of bile salts impact on physical properties of nisoldipine loaded bilosomes. Pharmacia. 2024 Feb;71(4):1-7. doi: 10.3897/pharmacia.71.e116917.
41. Sharma G, Sharma A. Recent insights on drug delivery system in hypertension: from bench to market. Curr Hypertens Rev. 2023;19(2):93-105. doi: 10.2174/1573402119666230707120846, PMID 37550916.
42. Varia U, Joshi D, Jadeja M, Katariya H, Detholia K, Soni V. Development and evaluation of ultra deformable vesicles loaded transdermal film of boswellic acid. Futur J Pharm Sci. 2022;8(1):39. doi: 10.1186/s43094-022-00428-2.
43. Fitri AM, Elim D, Mahfud MASB, Sultan NAF, Saputra MD, Afika N. Polymeric hydrogel-forming microneedle mediated transdermal delivery of sildenafil citrate from direct compressed tablet reservoir for potential improvement of pulmonary hypertension therapy. International Journal of Pharmaceutics. 2023 Jan 25;631:122549. doi: 10.1016/j.ijpharm.2021.122549.
44. Khatoon K, Rizwanullah M, Amin S, MIR SR, Akhter S. Cilnidipine loaded transfersomes for transdermal application: formulation optimization *in vitro* and *in vivo* study. J Drug Deliv Sci Technol. 2019;54:101303. doi: 10.1016/j.jddst.2019.101303.
45. Dudhipala N, Phasha Mohammed R, Adel Ali Youssef A, Banala N. Effect of lipid and edge activator concentration on development of aceclofenac loaded transfersomes gel for transdermal application: *in vitro* and ex vivo skin permeation. Drug Dev Ind Pharm. 2020;46(8):1334-44. doi: 10.1080/03639045.2020.1788069, PMID 32598194.
46. Mazhar D, Haq NU, Zeeshan M, Ain QU, Ali H, Khan S. Preparation characterization and pharmacokinetic assessment of metformin HCl loaded transfersomes co-equipped with permeation enhancer to improve drug bioavailability via transdermal route. J Drug Deliv Sci Technol. 2023 Jun;84:104448. doi: 10.1016/j.jddst.2023.104448.
47. Mahmood S, Chatterjee B, Mandal UK. Pharmacokinetic evaluation of the synergistic effect of raloxifene loaded transfersomes for transdermal delivery. J Drug Deliv Sci Technol. 2021;63:102545. doi: 10.1016/j.jddst.2021.102545.
48. Majukar S, Dandagi P, Kurangi B. Design and characterization of transfersomal patch of aceclofenac as a carrier for transdermal delivery. IOSR JPBS. 2019;9(1):1138-47. doi: 10.9790/3008-090103113847.
49. Sapkota R, Dash AK. Liposomes and transferosomes: a breakthrough in topical and transdermal delivery. Ther Deliv. 2021;12(2):145-58. doi: 10.4155/tde-2020-0122, PMID 33583219.
50. Oyarzun P, Gallardo Toledo E, Morales J, Arriagada F. Transfersomes as alternative topical nanodosage forms for the treatment of skin disorders. Nanomedicine. 2021;16(27):2465-89. doi: 10.2217/nnm-2021-0335.
51. Patil P, Nene S, Shah S, Singh SB, Srivastava S. Exploration of novel drug delivery systems in topical management of osteoarthritis. Drug Deliv Transl Res. 2023;13(2):531-46. doi: 10.1007/s13346-022-01229-z, PMID 36031671.
52. Lin SY. Thermoresponsive gating membranes embedded with liquid crystal(s) for pulsatile transdermal drug delivery: an overview and perspectives. J Control Release. 2020;319:450-74. doi: 10.1016/j.jconrel.2019.12.046, PMID 31901369.
53. Yuan M, Niu J, Xiao Q, YA H, Zhang Y, Fan Y. Hyaluronan modified transfersomes based hydrogel for enhanced transdermal delivery of indomethacin. Drug Deliv. 2022;29(1):1232-42. doi: 10.1080/10717544.2022.2053761, PMID 35403516.
54. Ruan J, Liu C, Song H, Zhong T, Quan P, Fang L. Sustainable and efficient skin absorption behaviour of transdermal drug: the effect of the release kinetics of permeation enhancer. Int J Pharm. 2022;612:121377. doi: 10.1016/j.ijpharm.2021.121377, PMID 34915145.
55. Altun E, Yuca E, Ekren N, Kalaskar DM, Ficai D, Dolete G. Kinetic release studies of antibiotic patches for local transdermal delivery. Pharmaceutics. 2021;13(5):613. doi: 10.3390/pharmaceutics13050613, PMID 33922739.
56. Shivalingam MR, Balasubramanian A, Ramalingam K. Formulation and evaluation of transdermal patches of pantoprazole sodium. Int J App Pharm. 2021;13(5):287-91. doi: 10.22159/ijap.2021v13i5.42175.
57. Matharoo N, Mohd H, Michniak Kohn B. Transferosomes as a transdermal drug delivery system: dermal kinetics and recent developments. Wiley Interdiscip Rev Nanomed Nanobiotechnol. 2024;16(1):e1918. doi: 10.1002/wnan.1918, PMID 37527953.
58. Jatav VS, Saggu JS, Sharma AK, Sharma A, Jat RK. Design development and permeation studies of nebivolol hydrochloride from novel matrix-type transdermal patches. Adv Biomed Res. 2013;2(1):62. doi: 10.4103/2277-9175.115813, PMID 24223377.
59. Deng P, Athary Abdulhaleem MF, Masoud RE, Alamoudi WM, Zakaria MY. Employment of PEGylated ultra deformable transferosomes for transdermal delivery of tapentadol with boosted bioavailability and analgesic activity in post-surgical pain. Int J Pharm. 2022 Nov 25;628:122274. doi: 10.1016/j.ijpharm.2022.122274, PMID 36228884.
60. Patel RP, Patel G, Baria A. Formulation and evaluation of transdermal patch of aceclofenac. Int J Drug Del. 2009 Jul;1(1):41-51. doi: 10.5138/ijdd.2009.0975.0215.01005.
61. Gannu R, Vamshi Vishnu Y, Kishan V, Madhusudan Rao Y. Development of nitrendipine transdermal patches: *in vitro* and ex vivo characterization. Curr Drug Deliv. 2007;4(1):69-76. doi: 10.2174/156720107779314767.
62. Parhi R, Padilam S. *In vitro* permeation and stability studies on developed drug-in-adhesive transdermal patch of simvastatin. Bull Fac Pharm Cairo Univ. 2018;56(1):26-33. doi: 10.1016/j.bfopcu.2018.04.001.
63. Tawfeek HM, Abdellatif AA, Abdel Aleem JA, Hassan YA, Fathalla D. Transfersomal gel nanocarriers for enhancement the permeation of lornoxicam. J Drug Deliv Sci Technol. 2020;56:101540. doi: 10.1016/j.jddst.2020.101540.
64. Gupta R, Kumar A. Transfersomes: the ultra deformable carrier system for non-invasive delivery of drug. Curr Drug Deliv. 2021;18(4):408-20. doi: 10.2174/1567201817666200804105416.
65. Bindu H, Radha. Design and *in vivo* evaluation of naproxen-loaded transferosomal gel for transdermal delivery. Int J App Pharm. 2024;16(2):272-84. doi: 10.22159/ijap.2024v16i2.49562.
66. Tiwari G, Tiwari R, Singh R, Rai AK. Ultra-deformable liposomes as flexible nanovesicular carrier to penetrate versatile drugs transdermally. NANOASIA. 2020;10(1):12-20. doi: 10.2174/2210681208666180820145327.
67. Nayak D, Tippavajhala VK. A comprehensive review on preparation, evaluation and applications of deformable liposomes. Iran J Pharm Res. 2021;20(1):186-205. doi: 10.22037/ijpr.2020.112878.13997, PMID 34400952.
68. Badr Eldin SM, Ahmed OA. Optimized nano transfersomal films for enhanced sildenafil citrate transdermal delivery: ex vivo and *in vivo* evaluation. Drug Des Dev Ther. 2016 Apr 5;10:1323-33. doi: 10.2147/DDDT.S103122.
69. Abdallah MH, Abu Lila AS, Shawky SM, Almansour K, Alshammari F, Khafagy ES. Experimental design and optimization of nano-transfersomal gel to enhance the hypoglycemic activity of silymarin. Polymers. 2022;14(3):508. doi: 10.3390/polym14030508, PMID 35160498.

70. Gayathri H, Sangeetha S. Design and development of tofacitinib citrate loaded transferosomal gel for skin cancer by box-behnken design doe approach. Int J Health Sci. 2022;6:3119-40. doi: 10.53730/ijhs.v6nS6.10118.
71. Rajpurohit M, Patil A, MV, Urolagin D, Saeed M, Ahmad I. Fabrication and characterisation of nabumetone transferosomal gel for effective topical delivery. J Mol Struct. 2024 Sep 15;1312:138430. doi: 10.1016/j.molstruc.2024.138430.
72. Das B, Nayak AK, Mallick S. Thyme oil containing fluconazole loaded transferosomal bigel for transdermal delivery. AAPS Pharm Sci Tech. 2023;24(8):240. doi: 10.1208/s12249-023-02698-2, PMID 37989918.